Soft Matter

RSC Publishing

PAPER

View Article Online
View Journal | View Issue

Published on 10 April 2013. Downloaded by University of Maryland - College Park on 04/06/2013 19:19:53.

Cite this: *Soft Matter*, 2013, **9**, 5025

A simple route to fluids with photo-switchable viscosities based on a reversible transition between vesicles and wormlike micelles†

Hyuntaek Oh,‡[a] Aimee M. Ketner,‡[a] Romina Heymann,[b] Ellina Kesselman,[c] Dganit Danino,[c] Daniel E. Falvey[b] and Srinivasa R. Raghavan*[ab]

Received 8th January 2013
Accepted 14th March 2013

DOI: 10.1039/c3sm00070b

www.rsc.org/softmatter

Recently, there has been much interest in photorheological (PR) fluids, *i.e.*, fluids whose rheological properties can be tuned by light. In particular, there is a need for simple, low-cost PR fluids that can be easily created using inexpensive, commercially available ingredients and that show substantial, *reversible* changes in rheology upon exposure to different wavelengths of light. Towards this end, we report a class of photoreversible PR fluids prepared by combining the azobenzene derivative 4-azobenzene carboxylic acid (ACA) (in its salt form) with the cationic surfactant erucyl bis(2-hydroxyethyl)methyl ammonium chloride (EHAC). We show that certain aqueous mixtures of EHAC and ACA, which are low-viscosity solutions at the outset, undergo nearly a *million-fold* increase in viscosity when irradiated with UV light. The same solutions revert to their initial viscosity when subsequently exposed to visible light. Using an array of techniques including UV-vis and NMR spectroscopies, small-angle neutron scattering (SANS) and cryo-transmission electron microscopy (cryo-TEM), we have comprehensively characterized these PR fluids at the molecular, nanostructural, and macroscopic scales. Initially, EHAC–ACA are self-assembled into unilamellar *vesicles*, which are discrete container structures and give the sample a low viscosity. Upon exposure to UV light, ACA undergoes a *trans* to *cis* photoisomerization, which alters the geometry of the EHAC–ACA complex. In turn, the molecules self-assemble into a different structure, *viz. wormlike micelles*, which are long, entangled chains and impart a high viscosity to the sample. The above changes in viscosity are repeatable, and the sample can be reversibly cycled back and forth between low and high viscosity states. Our photoreversible PR fluids can be easily replicated in any industrial or academic lab, and it is hoped that these "smart" fluids will eventually find a host of applications.

Introduction

Scientists have recently exhibited a growing interest in "smart" fluids or materials, *i.e.*, those that undergo a macroscopic change in property in response to an external stimulus.[1,2] A stimulus of particular interest has been light. Compared to other stimuli such as temperature, pH, or electric fields, light has many advantages.[3,4] Light can be directed from a distance at a precise location (with micron-scale resolution), and light sources at distinct wavelengths are widely available. A range of light-responsive "smart" materials are being studied, and one set of material properties that researchers are looking to modulate are the rheological or flow properties, such as viscosity.[2,5,6] Fluids with light-tunable rheology can be termed photorheological (PR) fluids.[5,7] Due to the spatial selectivity of light, PR fluids may be particularly useful in microscale or nanoscale devices such as microrobots,[8] lab-on-a-chip devices,[9] or as micropatternable biomaterials.[10] For many applications, reversibility of the PR effect is key, *i.e.*, the fluid should be capable of being cycled between low and high viscosity states by exposure to different wavelengths of light. For example, reversible PR fluids could be useful in recirculating systems[11] if they could be switched between a state enabling drag-reduction and one that permits rapid heat transfer.

A variety of PR fluids have been developed so far, but they have mostly relied on new, original classes of photoresponsive organic molecules that were synthesized in the laboratory. These molecules have typically consisted of a photoresponsive moiety attached to either a surfactant,[6,12–14] a polymer,[15–19] an

[a]*Department of Chemical and Biomolecular Engineering, University of Maryland, College Park, MD 20742-2111, USA. E-mail: sraghava@umd.edu*

[b]*Department of Chemistry & Biochemistry, University of Maryland, College Park, MD 20742, USA*

[c]*Department of Biotechnology and Food Engineering, Technion – Israel Institute of Technology, Haifa, 32000, Israel*

† Electronic supplementary information (ESI) available. See DOI: 10.1039/c3sm00070b

‡ Equal contribution.

Published on 10 April 2013. Downloaded by University of Maryland - College Park on 04/06/2013 19:19:53.

organogelator[10,20–25] or other species.[26,27] While these past approaches have demonstrated impressive PR effects, it is not straightforward for other researchers to replicate these results. Synthesis of such organic molecules can be costly and time-consuming; moreover, it is not clear if the molecules can be generated in sufficiently large quantities for exploring applications. The lack of simple, low-cost PR systems has provided the motivation for our work. We have deliberately chosen to emphasize the design of PR fluids using only commercially available molecules or particles.[28–33] Our goal has been to make PR systems that can be easily recreated by scientists in both academia and industry without investing time and effort in organic synthesis. In turn, wider availability is likely to spur on the search for new applications for these fluids.

Over the last five years, we have reported several examples of such simple PR fluids, including both aqueous[28–31] and organic[32,33] systems. We have been able to show that dramatic (>1000-fold) rheological changes can be triggered by light in simple systems. However, most of these PR fluids only allowed for their rheological properties to be changed in one direction (high to low, or low to high) by exposure to UV light; *i.e.*, the PR effect was not reversible.[28–30,32] There do exist a few simple systems that have demonstrated modest (10-fold) photoreversible viscosity change upon exposure to different wavelengths of light.[33–35] However, there is still very much a need for simple PR fluids that exhibit much larger (>1000-fold) photoreversible rheological changes.

In this paper, we describe a class of aqueous PR fluids that exhibit dramatic (million-fold) photoreversible viscosity changes. The fluids are composed of two commercially available components: an azobenzene derivative, 4-azobenzene carboxylic acid (ACA) and the cationic surfactant, erucyl bis(2-hydroxyethyl)methyl ammonium chloride (EHAC).[36] Chemical structures of these molecules are shown in Fig. 1. The PR effect occurs for certain molar ratios of EHAC and ACA, and for these samples exposure to UV light causes a *trans* to *cis* photoisomerization of ACA, which is accompanied by an increase in viscosity. Thereafter, when the sample is exposed to visible light, a *cis* to *trans* reverse photoisomerization of ACA occurs, and in turn the viscosity decreases to its initial value. We will show that the rheological changes correspond to a change in self-assembled structure, as indicated in Fig. 1: *i.e.*, the low-viscosity state corresponds to discrete unilamellar vesicles while the high-viscosity state corresponds to entangled wormlike micelles. The above changes in structure and hence rheology can be repeated, and the sample can be cycled between low and high viscosity states. We believe the above PR fluids can serve as a simple, workhorse system for use by academic and industrial researchers.

Results and discussion

The reversible PR fluids described here are aqueous mixtures of the cationic surfactant EHAC and the azobenzene-containing acid ACA, with base (NaOH) added to convert the ACA to its salt form (the NaOH is at a 10% molar excess relative to the ACA). We use the abbreviation ACA to refer to its *trans* dominant form,

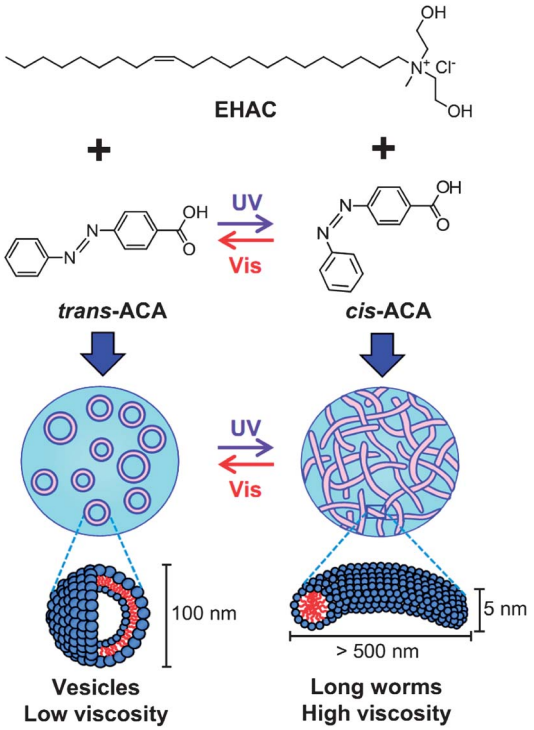

Fig. 1 Composition and mechanism of reversible PR fluids. The fluids are composed of the cationic surfactant EHAC and the azobenzene derivative ACA. When ACA is in its *trans* from, its mixture with EHAC forms discrete unilamellar vesicles that yield a low viscosity. Upon UV irradiation, *trans* ACA is photoisomerized to *cis* ACA, and in turn, entangled wormlike micelles are formed, which have a much higher viscosity. Upon subsequent irradiation with visible light, *cis* ACA is isomerized back to *trans* ACA, and the structure and rheology revert to their initial state.

which is the commercially available one. Only certain EHAC–ACA mixtures show substantial PR effects and these correspond to a distinct nanostructure. To illustrate this point, we first describe the phase behavior, rheology, and nanostructure of EHAC–ACA mixtures at a fixed [EHAC] of 40 mM. A 40 mM solution of EHAC alone has a viscosity close to water. When ACA salt is added, the carboxylate anions bind to the cationic headgroups of EHAC, and this leads to the growth of long wormlike micelles, which entangle and thereby viscosify the solution. Accordingly, the zero-shear viscosity η_0 of EHAC–ACA solutions increases by 5 orders of magnitude with increasing [ACA] and reaches a maximum around 14 mM ACA (see Fig. S1b, ESI†). Solutions between 10 and 16 mM ACA show strong viscoelasticity and flow-birefringence, as is typical of wormlike micelles (see photographs in Fig. S1†).[37]

Beyond 14 mM, further increase in [ACA] causes the viscosity to plummet (Fig. S1b†). For [ACA] > 18 mM, η_0 plateaus at a value ~3 mPa s, which is 3 times the viscosity of water. A peak in η_0 as a function of salt concentration is frequently seen in wormlike micellar systems and is thought to signify a transition from linear to branched wormlike micelles.[36–38] But the viscosity plateau for [ACA] > 18 mM is unusual, and samples in this region have features that are distinct from micelles. These low-viscosity samples also have a high optical density (turbidity), as shown by Fig. S1a,† indicating the presence of larger objects

 This journal is © The Royal Society of Chemistry 2013

Published on 10 April 2013. Downloaded by University of Maryland - College Park on 04/06/2013 19:19:53.

that scatter light.[39] Note that the onset of turbidity and the viscosity plateau both occur around 20 mM ACA (Fig. S1†). Photographs of a typical sample in this region are shown in Fig. S1† and we note that the sample is turbid but homogeneous; also there is no flow-birefringence. These data are indicative of a phase transition from micelles to vesicles in EHAC–ACA mixtures with increasing ACA concentration.[39,40] Support for the presence of wormlike micelles at moderate [ACA] and vesicles at higher [ACA] are provided by data from small-angle neutron scattering (SANS) and cryo-transmission electron microscopy (cryo-TEM). These data are discussed below in Fig. 2 and complementary sets of data are shown in Fig. S2.† Similar micelle-to-vesicle transitions in mixtures of a cationic surfactant and an organic salt are rare, but have been noted in a couple of previous studies.[39,40]

The samples that show large, reversible PR effects are those corresponding to the vesicle region in Fig. S1.† We will discuss typical photorheological results for a sample containing 40 mM EHAC, 20 mM ACA, and 22 mM NaOH. First, we confirmed by UV-vis spectroscopy that the ACA in this sample does undergo a reversible photoisomerization in the presence of EHAC. As shown by Fig. S3,† the initial sample has two absorption bands: a main peak at 323 nm, corresponding to a π–π* excitation, and a secondary peak at 444 nm, corresponding to an n–π* excitation.[41] Upon 1 h irradiation with broadband (300–350 nm) UV light, the peak at 323 nm drops by 25.3% and concomitantly the peak at 444 nm increases by 68.6% (Fig. S3,† inset), which together indicate a *trans* to *cis* photoisomerization of ACA. (The photostationary state was reached after 2 h of UV irradiation, and corresponded to a 28.3% drop of the peak at 323 nm.) Subsequent irradiation with visible light (400–450 nm) for 1.5 h causes a complete reversion of the spectrum to its original values – *i.e.*, the peak at 323 nm grows back while the peak at 444 nm drops. Together, these data confirm that visible light induces the reverse *cis* to *trans* photo-isomerization.[41]

We now discuss the effect of UV- and visible-light irradiation on the rheology of the 40 mM EHAC, 20 mM ACA, and 22 mM NaOH sample. As shown by Photo 1 in Fig. 2a, this sample is initially turbid with an orange color and it is water-like in its viscosity – it thus flows readily out of the tilted vial. When the

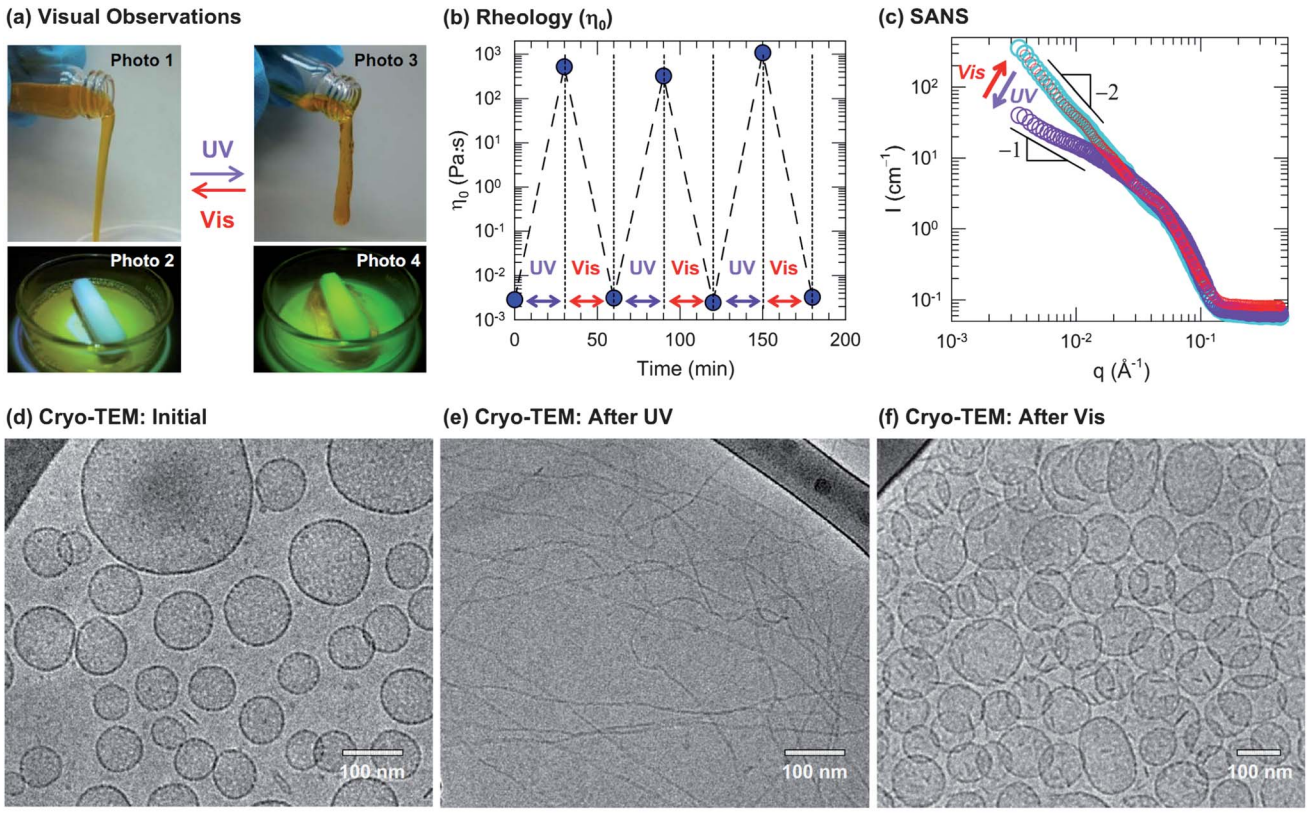

Fig. 2 Reversible photorheological response and its nanostructural origin. A sample containing 40 mM EHAC, 20 mM ACA, and 22 mM NaOH was used for (a), (b) and (d)–(f). (a) Visual observations illustrate the dramatic light-induced changes in fluid properties: initially, the sample is a cloudy, water-like fluid (Photo 1 and 2) whereas UV light transforms it into a transparent viscoelastic and gel-like fluid that shows the tubeless siphon (Photo 3) and rod climbing (Photo 4) effects. This is reversed by irradiation with visible light. (b) The rheology is quantified in terms of the zero-shear viscosity η_0. The data show that the sample can be cycled between low and high viscosity states (10^5-fold difference) by repeated UV and visible light irradiation. (c) SANS spectra on a diluted sample in D_2O (10 mM EHAC, 6.5 mM ACA, and 7.2 mM NaOH) reveal a reversible light-induced transition between two types of self-assembled structures: initially, the intensity *I* follows a slope of −2 at low ***q*** (cyan circles), which is characteristic of vesicles at low ***q***. Upon UV irradiation, the slope is decreased and approaches −1 (violet circles), which is indicative of cylindrical (wormlike) micelles. Upon subsequent visible-light irradiation, the original spectrum is recovered (red circles). The above structural transition is confirmed by cryo-TEM. A typical image of the initial sample (d) reveals discrete unilamellar vesicles, whereas after UV irradiation (e) the sample is found to contain long, entangled wormlike micelles, and finally, after subsequent visible-light irradiation (f) the sample reverts to the vesicle state.

Published on 10 April 2013. Downloaded by University of Maryland - College Park on 04/06/2013 19:19:53.

sample is stirred, the magnetic stir bar rotates smoothly and the fluid does not stick to the bar (Photo 2). Upon UV irradiation, the sample gradually becomes more transparent and viscous. The irradiated sample resists flow out of the tilted vial, and when it does flow, it moves as one mass (Photo 3) – this is a phenomenon associated with viscoelastic fluids called the "tubeless siphon" effect.[42,43] This sample is also flow-birefringent, and when bubbles are introduced in it, they remain trapped for long times. Also, during UV irradiation under stirring, the sample gradually gathers and sticks to the stir bar (Photo 4) – this is a manifestation of the "rod climbing" effect.[42] Taken together, it is clear that the UV-irradiated sample is highly viscoelastic, as is typical of wormlike micellar systems.[37] Subsequent irradiation with visible light reverts the sample to its original properties. The sample is converted back to a thin, runny fluid that can be poured easily out of the vial.

The above visual observations are quantified through steady-shear (Fig. 3) and dynamic (Fig. 4) rheological measurements. From steady-shear rheology, the initial sample is seen to have a low viscosity (3 mPa s) that is nearly independent of shear rate, indicating Newtonian behavior (Fig. 3). Correspondingly, the sample shows a purely viscous response in dynamic rheology: *i.e.*, the viscous modulus G'' is strongly dependent on frequency ω whereas the elastic modulus G' is too low to be detected (Fig. 4a). Upon UV irradiation, the sample becomes non-Newtonian and shear-thinning – the viscosity shows a plateau value $\eta_0 \sim 500$ Pa s at low shear-rates and decreases at higher shear-rates (Fig. 3). In turn, the dynamic rheological response is strongly viscoelastic (Fig. 4b): *i.e.*, the response is elastic at high frequencies or short timescales ($G' > G''$) and viscous at low frequencies or long timescales ($G'' > G'$).[42] Finally, upon subsequent visible-light irradiation, both the steady and dynamic rheological responses revert to their initial cases (Fig. 3 and 4c).

To measure the cyclability of the photorheological response, we characterize the sample by its zero-shear viscosity η_0. Fig. 2b plots the values of η_0 under repeated UV and visible light irradiation for 30 min each. The data show that η_0 can be repeatedly cycled between a low value of 3 mPa s and a high value around 500 Pa s, *i.e.*, $a > 10^5$-fold change. The magnitude of the response remains identical even after 3 full cycles, *i.e.*, there is no fatigue or deterioration in the response. During these cycling tests, repeated photoisomerization between *trans* and *cis* ACA was confirmed by UV-vis: we found a 21% drop of the absorbance at 323 nm after 30 min of UV and complete recovery to the initial absorbance after visible light irradiation for each of the 3 cycles.

Fig. 2 also presents results from SANS and cryo-TEM confirming that the PR effects are due to a reversible vesicle–micelle transition. First, we show data from SANS for the intensity *I vs.* scattering vector $\boldsymbol{q}$ in Fig. 2c. These data were obtained on a diluted sample (10 mM EHAC/6.5 mM ACA/7.2 mM NaOH) to minimize structure factor effects. Initially, this sample shows a $\boldsymbol{q}^{-2}$ decay of the intensity at low $\boldsymbol{q}$, which is characteristic of vesicles.[44] After 1 h of UV irradiation, a significant drop occurs in the intensity at low $\boldsymbol{q}$ and the intensity asymptotes to a slope close to -1 at low $\boldsymbol{q}$, which is indicative of long, cylindrical micelles.[44] Next, after 1.5 h of visible-light irradiation, the SANS data perfectly overlap with that of the sample before irradiation.

Fig. 2d–f present cryo-TEM images of the 40 mM EHAC, 20 mM ACA, and 22 mM NaOH sample. As expected, the sample initially contains mostly unilamellar vesicles (Fig. 2d). The vesicles have diameters between ~80 and 200 nm, and their surfaces appear to be perforated rather than smooth. In some

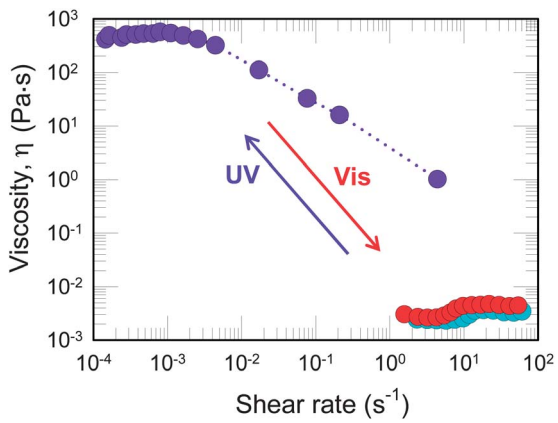

Fig. 3 Steady-shear rheology of a sample of 40 mM EHAC, 20 mM ACA, and 22 mM NaOH. Data for the apparent viscosity *vs.* shear rate are shown for the initial sample (cyan circles), after UV irradiation for 30 min (purple circles), and after subsequent visible light irradiation for 30 min (red circles).

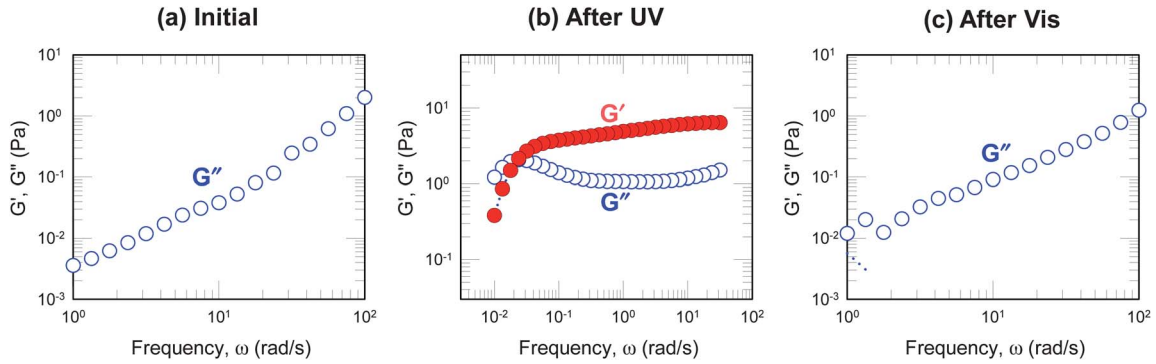

Fig. 4 Dynamic rheology of a sample of 40 mM EHAC, 20 mM ACA, and 22 mM NaOH. Data for the elastic modulus G' and the viscous modulus G'' as functions of frequency ω are shown for the initial sample (a), after UV irradiation for 30 min (b), and after subsequent visible light irradiation for 30 min (c).

 This journal is © The Royal Society of Chemistry 2013

Published on 10 April 2013. Downloaded by University of Maryland - College Park on 04/06/2013 19:19:53.

images, we also observed coexistence of such vesicles with a few wormlike micelles (Fig. S2b and c†). The perforated vesicles are evidently transitional structures between micelles and vesicles, and they have been observed in the transition regions between micelle and vesicle phases in other surfactant systems.[45,46] Next, we consider the sample after UV irradiation, and its cryo-TEM images clearly show the presence of long, entangled wormlike micelles,[37] as can be noted from the typical image in Fig. 2e. The worms are seen to have a diameter <5 nm whereas their contour (end-to-end) lengths extend up to a micron or more. These worms are responsible for the UV-induced increase in visco-elasticity (also the much smaller diameter of the worms relative to the vesicles explains why the latter solutions are much more turbid than the former). Finally, visible-light irradiation brings the structure back to perforated vesicles, as seen in Fig. 2f. Overall, cryo-TEM, SANS, visual observations, and rheology are all in agreement in attributing the PR effect to a transition between unilamellar vesicles and wormlike micelles.

Fig. 5 plots the influence of sample composition on the PR effect. This was studied at a constant [EHAC] of 40 mM and varying [ACA]. Data are shown for the zero-shear viscosity η_0 of the samples before irradiation, following UV irradiation, and following subsequent visible-light irradiation. This plot shows that the PR effect is significant only for samples in the "vesicle" region, *i.e.*, [ACA] > 18 mM, which fall to the right of the viscosity peak. For these samples, 1 h of UV irradiation increased η_0 by up to 6 orders of magnitude (million-fold). Specifically, the sample at an [ACA] of 20 mM shows a 1.4 million-fold increase in η_0. Subsequent visible-light irradiation for 1.5 h brought η_0 back to nearly its original value. Note that samples to the left of the viscosity peak do not show any significant PR effects.

A final piece of this puzzle is to explain how *trans* and *cis* ACA lead to different self-assembled structures, *i.e.*, vesicles and worms, respectively. To address this issue, we collected ^{1}H NMR spectra on EHAC–ACA mixtures in D_2O at a fixed EHAC concentration of 10 mM. Fig. 6a and b represent the chemical shifts of the ring protons of ACA before and after UV irradiation, respectively. The protons corresponding to each peak are shown in Fig. 6c and d. The chemical shift difference $\Delta\delta$ of the protons is indicative of the environment surrounding the molecules.[47–50] An upfield shift indicates a higher electron density of the environment; this occurs when aromatic protons are in the hydrophobic interior of micelles or vesicles and the magnitude of $\Delta\delta$ reflects the insertion depth of these protons.[47–50] On the contrary, a downfield shift indicates a lower electron density of the environment; this occurs when the protons are near the surface of the micelles or vesicles and thereby close to the charged headgroups of the surfactant.[47–50]

The ^{1}H NMR spectra of ACA before UV irradiation show three groups of peaks for each *trans* and *cis* form, as seen in Fig. 6a. The ratio of *cis* to *trans* ACA is 0.24 (80.6% *trans* and 19.4% *cis*), obtained by integrating the corresponding peaks of a control sample. Each group of peaks shows different shifts in the presence of 10 mM EHAC. At an ACA concentration of 6.5 mM, the peaks d and e experience the largest upfield shift $\Delta\delta$ (−0.46 ppm), which suggests that these protons are the farthest from the headgroup of EHAC. Peaks b and c show a $\Delta\delta \sim -0.19$ ppm while the peaks of a show a negligible $\Delta\delta \sim -0.02$ ppm. Although the $\Delta\delta$ for these three groups keep changing with [ACA], their order is very consistent, *i.e.*, in magnitude, a < b, c < d, e. This suggests that the *trans* ACA is inserted vertically into the micelles or vesicles.[47–51] Note that the broadening of signals at higher [ACA] is due to the binding of ACA to the micelles or vesicles rather than an increased viscosity of solution.

After UV irradiation, the intensity of peaks corresponding to the *cis* form increases whereas that of the *trans* form decreases, as seen in Fig. 6b. The *cis* to *trans* ratio of ACA without EHAC after 30 min UV irradiation is 2.26 (30.7% *trans* and 69.3% *cis*). However, the *cis* to *trans* ratio of ACA after 1 h UV irradiation in the presence of 10 mM EHAC is 0.60 (62.6% *trans* and 37.4% *cis*) obtained by integrating peaks corresponding to d, e and d′, e′. Although there is some inaccuracy due to peak broadening, this result is consistent with our UV-vis data in showing that ACA photoisomerization is somewhat restricted when ACA is bound to EHAC. Now, consider the $\Delta\delta$ values for 6.5 mM ACA after UV irradiation. Notably, the $\Delta\delta$ of a′ (−0.01 ppm), b′ and c′ (−0.3 ppm) are all close to the corresponding protons of the *trans* form; however, $\Delta\delta$ of d′ and e′ is −0.3 ppm, which is quite different from that of protons d and e (−0.46 ppm) of *trans* ACA. The smaller magnitude of $\Delta\delta$ for d′ and e′ implies that these protons are shifted toward the interface of the EHAC aggregates. That is, when *trans* ACA is converted to *cis* ACA, the phenyl group far from the carboxylate is induced to move upward,[47–50] as shown in Fig. 6c and d.

Fig. 6c and d present the most reasonable arrangement of *trans* and *cis* ACA in the EHAC–ACA aggregates, as per the NMR data. The impact of these geometric differences on self-assembly can be rationalized using the concept of the critical packing parameter $p = a_{tail}/a_{head}$, *i.e.*, p is the ratio of the average area of the tail portion (a_{tail}) to the average area of the head portion (a_{head}).[52,53] In the case of EHAC and *trans* ACA (Fig. 6c), the azobenzene group of ACA is embedded vertically and adjacent to the tail of EHAC while the carboxylate anion of ACA is next to the cationic headgroups of EHAC at the interface.

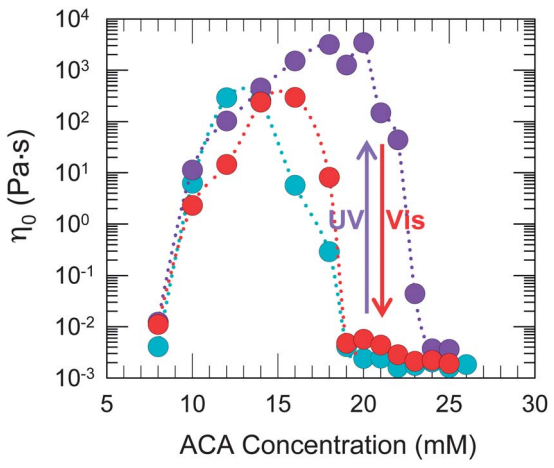

Fig. 5 Influence of sample composition on the PR effect. The zero-shear viscosity η_0 is plotted for samples at constant [EHAC] of 40 mM and varying [ACA] for three cases: initial, *i.e.*, before any irradiation (cyan circles); after 1 h of UV irradiation (violet circles); and after subsequent 1.5 h of visible-light irradiation (red circles).

Published on 10 April 2013. Downloaded by University of Maryland - College Park on 04/06/2013 19:19:53.

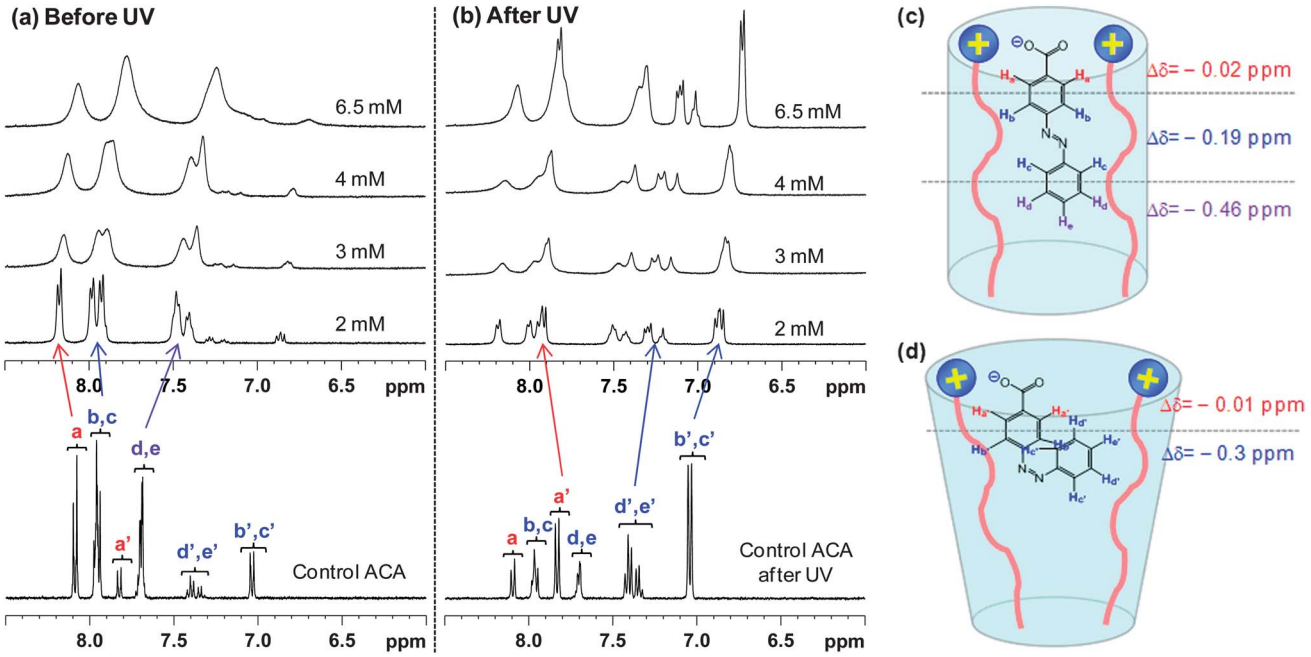

Fig. 6 Molecular arrangement of *trans* and *cis* ACA in the EHAC–ACA aggregates. ^{1}H NMR spectra of 2–6.5 mM ACA in 10 mM EHAC and 1 mM ACA in D_2O (control) are plotted: (a) before UV irradiation and (b) after 1 h of UV irradiation. The signals a–d correspond to the protons of *trans* ACA shown in the schematic structure (c). The signals a′, b′, c′, and d′ correspond to the protons of *cis* ACA shown in (d). (c) and (d) represent the most reasonable molecular arrangement of EHAC–ACA, which is inferred from the chemical shift differences ($\Delta\delta$) for *trans* ACA and *cis* ACA respectively.

The binding of anionic and cationic moieties reduces the electrostatic repulsions of the headgroup and a_{head} is thus maintained low. In effect, a_{head} and a_{tail} are comparable, *i.e.*, $p = 1$, so that the net molecular geometry is that of a cylinder (Fig. 6c). Such a p value implies the formation of vesicles.[52,53] When *trans* ACA is photoisomerized to *cis* ACA, the lower phenyl ring of *cis*

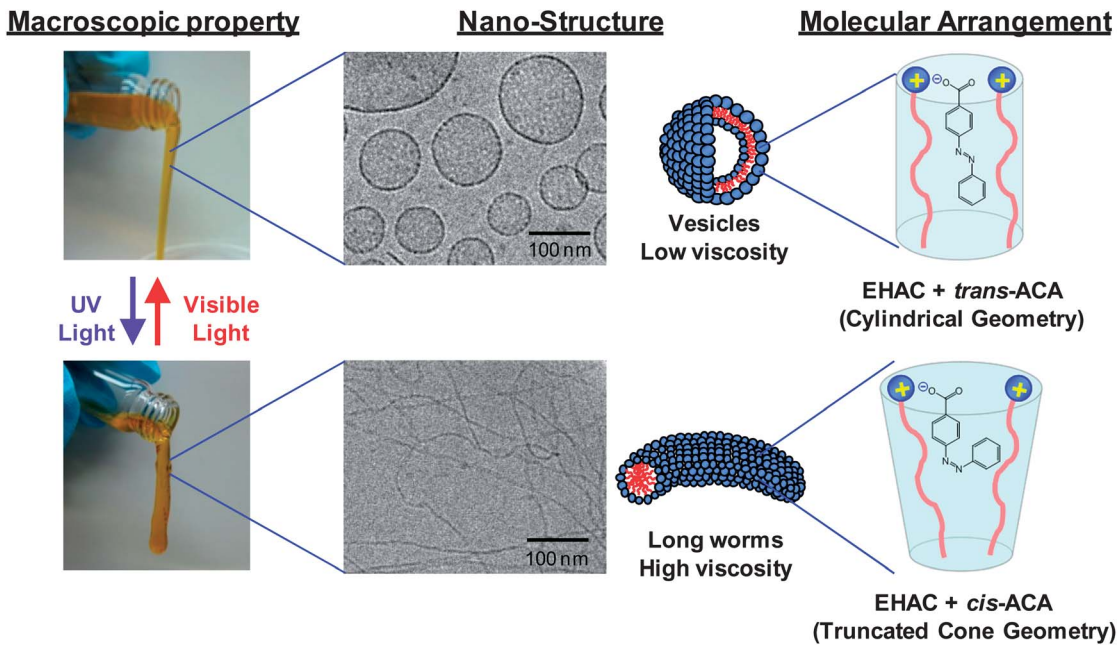

Fig. 7 Photoresponsive character of the EHAC–ACA system at the molecular, nanostructural, and macroscopic scales. At the molecular scale, initially *trans* ACA binds strongly to EHAC and the net molecular arrangement is in a cylindrical geometry, which results in self-assembly into unilamellar vesicles at the nanoscale, and thereby results in a freely flowing low-viscosity fluid at the macroscopic scale. When UV-irradiated, at the molecular scale, *trans* ACA is photoisomerized to *cis* ACA. The arrangement of *cis* ACA with EHAC is altered to a truncated-cone geometry, thus dictating self-assembly into long wormlike micelles at the nanoscale, and thereby producing a highly viscoelastic fluid at the macroscopic scale. Finally, exposure to UV light reverts the ACA back from *cis* to its *trans* isomer, and thereby reverts the nanostructure and rheology to their initial states.

 This journal is © The Royal Society of Chemistry 2013

Published on 10 April 2013. Downloaded by University of Maryland - College Park on 04/06/2013 19:19:53.

ACA is displaced toward the interface, which widens the gap between headgroups of EHAC, *i.e.*, a_{head} increases, while a_{tail} may not be altered as much.[54] In effect, there is a net decrease in p to a value closer to ½, which corresponds to a truncated cone geometry (Fig. 6d). Such a p value implies the formation of cylindrical structures such as wormlike micelles.[52,53] In sum, we have used NMR to infer a change in the overall geometry of EHAC–ACA aggregates upon photo-isomerization, which manifests as a transition between two types of self-assembled structures: vesicles and wormlike micelles.

Conclusions

We have demonstrated reversible light-induced rheological and structural transitions in solutions prepared from inexpensive and commercially available chemicals, *viz.* the cationic surfactant EHAC and the azobenzene derivative ACA. Fig. 7 summarizes our results and illustrates how the molecular structure dictates the nanostructure and in turn, the macroscopic properties. First, in the initial case, *trans* ACA binds strongly with EHAC, leading to a cylinder-like molecular geometry and thereby to unilamellar vesicles. This nanostructure corresponds to a low viscosity. When irradiated with UV light, *trans* ACA is photoisomerized to *cis* ACA, which is displaced towards the headgroup of EHAC, leading to a truncated-cone geometry. In turn, the vesicles rearrange into entangled wormlike micelles, which display a dramatically higher viscosity (increase in η_0 by up to a factor of 10^6). Upon subsequent visible-light irradiation, *cis* ACA reverts to *trans* ACA, and in turn, the self-assembled structure and viscosity revert to their original states. Among the available photorheological (PR) fluids, the EHAC–ACA system is particularly attractive because it can be easily prepared in any industrial or academic lab and because it exhibits a large PR response and complete photoreversibility. It is hoped that these "smart" fluids will eventually find applications in microscale or mesoscale devices. In addition to the PR response, light-activated vesicle rupture and formation in EHAC–ACA may also be useful for photo-controlled release of vesicle contents.[55,56]

Materials and methods

Materials

EHAC (ETHOQUAD® E/12-75) was received as a gift from Akzo Nobel.[36] The product is supplied by the manufacturer as a solution of 75% surfactant in isopropyl alcohol (IPA). The IPA was removed in a vacuum oven at room temperature and the surfactant was dried to constant weight. ACA (greater than 98% in purity, mostly in *trans* form) was purchased from TCI. Ultrapure deionized water from a Millipore water purification system was used in preparing samples. For the SANS and NMR studies, D_2O (99.95% deuterated, from Cambridge Isotopes) was used.

Sample preparation

Samples for rheological characterization and visual observation were prepared by dissolving weighed amounts of dried EHAC in ultrapure deionized water followed by the addition of desired amounts of ACA and 10% molar excess of sodium hydroxide (NaOH) to reach the final composition. Samples were stirred continuously around 40 °C for 5 hours to obtain homogeneous solutions. The solutions were stirred additionally for 1 day at room temperature and then left at rest to equilibrate for 3 days at room temperature before any experiments were conducted. The pH of the samples was between 6 and 7. For SANS studies, samples were prepared in D_2O using EHAC, ACA and NaOH and with the same preparation procedure. For NMR studies, samples were similar to the above, but NaOH was replaced with sodium deuteroxide (NaOD).

Sample response before and after UV irradiation

EHAC–ACA samples were irradiated with UV light from an Oriel 200 W mercury arc lamp. A dichroic beam turner with a mirror reflectance range of 350 to 450 nm was used to access the desired UV range of the emitted light. We used a filter for < 400 nm light to filter out the undesired visible wavelengths for the forward irradiation, and a filter for > 400 nm light to filter out the undesired UV wavelengths for the reverse irradiation. Samples (2.5 mL) were placed in a Petri dish with a quartz cover, and irradiation was done for a specific duration under stirring. After UV irradiation, 1 mL of sample was taken out for UV-vis spectra and rheological measurements, and then consecutive visible light irradiation was done with the remaining 1.5 mL of the sample. Samples were covered with aluminum foil during storage to minimize undesired exposure to visible light. UV-vis spectroscopy before and after irradiation was carried out using a Varian Cary 50 spectrophotometer.

Rheological studies

Rheological experiments were performed on an AR2000 stress controlled rheometer (TA Instruments, Newark, DE). 1 hour equilibration time was introduced before rheological measurement after light irradiation. Samples were run at 25 °C on a cone-and-plate geometry (40 mm diameter, 2° cone angle).

SANS

SANS measurements were made on the NG-7 (30 m) beamline at National Institute of Standards and Technology (NIST) in Gaithersburg, MD. Neutrons with a wavelength of 6 Å were selected. Three sample-detector distances were used to probe a wide range of wave vectors from 0.004 to 0.4 $Å^{-1}$. Samples were studied in 2 mm quartz cells at 25 °C. The scattering spectra were corrected and placed on an absolute scale using calibration standards provided by NIST. The data are shown for the radially averaged intensity I as a function of the wave vector $\boldsymbol{q} = (4\pi/\lambda)\sin(\theta/2)$, where λ is the neutron wavelength and θ is the scattering angle.

Cryo-TEM

Specimens were prepared in a controlled environment vitrification system (CEVS) at 25 °C and 100% relative humidity.[57] A drop of solution was placed on a TEM grid covered with a perforated carbon film and blotted with a filter paper to form

Published on 10 April 2013. Downloaded by University of Maryland - College Park on 04/06/2013 19:19:53.

a thin film on the grid. The exact amount of blotting and its mode of application were adjusted so as to obtain films ranging between 100 and 250 nm in thickness. The blotted samples were allowed to stand in the CEVS for 10–30 s to relax from shearing effects caused by the blotting. The relaxed samples were then plunged into liquid ethane at its freezing temperature (−183 °C) to form vitrified specimens and stored at −196 °C in liquid nitrogen until examination. Specimens were examined in a Philips CM120 TEM optimized for cryo-TEM work. The microscope was operated at an accelerating voltage of 120 kV using an Oxford CT3500 cryo-specimen holder that maintained the vitrified specimens below −175 °C. Specimens were examined in the low-dose imaging mode to minimize electron-beam radiation damage. Images were recorded digitally at nominal magnifications up to 175 000× on a cooled Gatan MultiScan 791 CCD camera, using the Digital Micrograph software.

^{1}H NMR

^{1}H NMR spectra were taken on a Bruker AVANCE 400 MHz spectrometer, BBI probe. The 30° pulse sequence was the standard "zg30" from Bruker. Particulars of the program include relaxation delay of 2 s, spectral width of 8012.82 Hz, and time domain 32768, giving a FID resolution of 0.244532 Hz. Spectra were processed on Topspin version 2.1 and referenced to the H_2O chemical shift signal of 4.8 ppm.

Acknowledgements

The work at UMD was funded by an NSF CAREER award, an EAGER grant from NSF-CBET and a grant from NIST. We acknowledge NIST NCNR for facilitating the SANS experiments performed as part of this work. Undergraduate students Reza Hashemipour, Nick Yaraghi and Patrick Elder, and graduate students Rakesh Kumar and Kunshan Sun provided valuable assistance in performing some of the experiments at UMD and their contributions are acknowledged. For the cryo-TEM work at the Technion, the financial support of the Israel Science Foundation (ISF) and the Russell-Berrie Nanotechnology Institute (RBNI) are acknowledged. We thank Dr Ludmila Abezgauz for superb assistance with the cryo-TEM experiments.

References

1 M. A. C. Stuart, W. T. S. Huck, J. Genzer, M. Muller, C. Ober, M. Stamm, G. B. Sukhorukov, I. Szleifer, V. V. Tsukruk, M. Urban, F. Winnik, S. Zauscher, I. Luzinov and S. Minko, *Nat. Mater.*, 2010, **9**, 101–113.
2 J. M. J. Paulusse and R. P. Sijbesma, *Angew. Chem., Int. Ed.*, 2006, **45**, 2334–2337.
3 K. G. Yager and C. J. Barrett, *J. Photochem. Photobiol. A*, 2006, **182**, 250–261.
4 Y. Zhao and T. Ikeda, *Smart Light-Responsive Materials: Azobenzene-Containing Polymers and Liquid Crystals*, Wiley, Hoboken, N.J., 2009.
5 T. Wolff and B. Klaussner, *Adv. Colloid Interface Sci.*, 1995, **59**, 31–94.
6 J. Eastoe and A. Vesperinas, *Soft Matter*, 2005, **1**, 338–347.
7 T. Wolff, C. S. Emming, T. A. Suck and G. Von Bunau, *J. Phys. Chem.*, 1989, **93**, 4894–4898.
8 S. W. Bates, Quantifying the stimuli of photorheological fluids, S. M. thesis, Massachusetts Institute of Technology, 2010.
9 S. R. Sershen, G. A. Mensing, M. Ng, N. J. Halas, D. J. Beebe and J. L. West, *Adv. Mater.*, 2005, **17**, 1366–1370.
10 S. Matsumoto, S. Yamaguchi, S. Ueno, H. Komatsu, M. Ikeda, K. Ishizuka, Y. Iko, K. V. Tabata, H. Aoki, S. Ito, H. Noji and I. Hamachi, *Chem.–Eur. J.*, 2008, **14**, 3977–3986.
11 H. F. Shi, Y. Wang, B. Fang, Y. Talmon, W. Ge, S. R. Raghavan and J. L. Zakin, *Langmuir*, 2011, **27**, 5806–5813.
12 C. T. Lee, K. A. Smith and T. A. Hatton, *Macromolecules*, 2004, **37**, 5397–5405.
13 H. Sakai, Y. Orihara, H. Kodashima, A. Matsumura, T. Ohkubo, K. Tsuchiya and M. Abe, *J. Am. Chem. Soc.*, 2005, **127**, 13454–13455.
14 B. L. Song, Y. F. Hu and J. X. Zhao, *J. Colloid Interface Sci.*, 2009, **333**, 820–822.
15 I. Tomatsu, A. Hashidzume and A. Harada, *J. Am. Chem. Soc.*, 2006, **128**, 2226–2227.
16 G. Pouliquen and C. Tribet, *Macromolecules*, 2006, **39**, 373–383.
17 S. Deshmukh, L. Bromberg, K. A. Smith and T. A. Hatton, *Langmuir*, 2009, **25**, 3459–3466.
18 Y. L. Zhao and J. F. Stoddart, *Langmuir*, 2009, **25**, 8442–8446.
19 D. Chen, H. Liu, T. Kobayashi and H. F. Yu, *J. Mater. Chem.*, 2010, **20**, 3610–3614.
20 K. Murata, M. Aoki, T. Suzuki, T. Harada, H. Kawabata, T. Komori, F. Ohseto, K. Ueda and S. Shinkai, *J. Am. Chem. Soc.*, 1994, **116**, 6664–6676.
21 S. Yagai, T. Nakajima, K. Kishikawa, S. Kohmoto, T. Karatsu and A. Kitamura, *J. Am. Chem. Soc.*, 2005, **127**, 11134–11139.
22 N. S. S. Kumar, S. Varghese, G. Narayan and S. Das, *Angew. Chem., Int. Ed.*, 2006, **45**, 6317–6321.
23 G. C. Kuang, Y. Ji, X. R. Jia, Y. Li, E. Q. Chen, Z. X. Zhang and Y. Wei, *Tetrahedron*, 2009, **65**, 3496–3501.
24 Y. P. Wu, S. Wu, X. J. Tian, X. Wang, W. X. Wu, G. Zou and Q. J. Zhang, *Soft Matter*, 2011, **7**, 716–721.
25 R. Rajaganesh, A. Gopal, T. M. Das and A. Ajayaghosh, *Org. Lett.*, 2012, **14**, 748–751.
26 Y. Y. Lin, X. H. Cheng, Y. Qiao, C. L. Yu, Z. B. Li, Y. Yan and J. B. Huang, *Soft Matter*, 2010, **6**, 902–908.
27 M. Pereira, C. R. Leal, A. J. Parola and U. M. Scheven, *Langmuir*, 2010, **26**, 16715–16721.
28 A. M. Ketner, R. Kumar, T. S. Davies, P. W. Elder and S. R. Raghavan, *J. Am. Chem. Soc.*, 2007, **129**, 1553–1559.
29 R. Kumar and S. R. Raghavan, *Soft Matter*, 2009, **5**, 797–803.
30 K. S. Sun, R. Kumar, D. E. Falvey and S. R. Raghavan, *J. Am. Chem. Soc.*, 2009, **131**, 7135–7141.
31 V. Javvaji, A. G. Baradwaj, G. F. Payne and S. R. Raghavan, *Langmuir*, 2011, **27**, 12591–12596.
32 R. Kumar, A. M. Ketner and S. R. Raghavan, *Langmuir*, 2010, **26**, 5405–5411.
33 H. Y. Lee, K. K. Diehn, K. S. Sun, T. H. Chen and S. R. Raghavan, *J. Am. Chem. Soc.*, 2011, **133**, 8461–8463.

 This journal is © The Royal Society of Chemistry 2013

Published on 10 April 2013. Downloaded by University of Maryland - College Park on 04/06/2013 19:19:53.

34 X. L. Yu and T. Wolff, *Langmuir*, 2003, **19**, 9672–9679.
35 A. Matsumura, K. Sakai, H. Sakai and M. Abe, *J. Oleo Sci.*, 2011, **60**, 203–207.
36 S. R. Raghavan and E. W. Kaler, *Langmuir*, 2001, **17**, 300–306.
37 C. A. Dreiss, *Soft Matter*, 2007, **3**, 956–970.
38 L. Ziserman, L. Abezgauz, O. Ramon, S. R. Raghavan and D. Danino, *Langmuir*, 2009, **25**, 10483–10489.
39 T. S. Davies, A. M. Ketner and S. R. Raghavan, *J. Am. Chem. Soc.*, 2006, **128**, 6669–6675.
40 L. Li, Y. Yang, J. F. Dong and X. F. Li, *J. Colloid Interface Sci.*, 2010, **343**, 504–509.
41 W. M. Horspool and F. Lenci, *CRC Handbook of Organic Photochemistry and Photobiology*, CRC Press, Boca Raton, 2nd edn, 2004.
42 C. W. Macosko, *Rheology: Principles, Measurements, and Applications*, Wiley-VCH, New York, 1994.
43 R. G. Larson, *The Structure and Rheology of Complex Fluids*, Oxford University Press, New York, Oxford, 1999.
44 J. S. Pedersen, *Adv. Colloid Interface Sci.*, 1997, **70**, 171–210.
45 R. Kakehashi, G. Karlsson and M. Almgren, *J. Colloid Interface Sci.*, 2009, **331**, 484–493.
46 M. Almgren, *Soft Matter*, 2010, **6**, 1383–1390.
47 S. J. Bachofer, U. Simonis and T. A. Nowicki, *J. Phys. Chem.*, 1991, **95**, 480–488.
48 S. J. Bachofer and U. Simonis, *Langmuir*, 1996, **12**, 1744–1754.
49 P. J. Kreke, L. J. Magid and J. C. Gee, *Langmuir*, 1996, **12**, 699–705.
50 M. Vermathen, P. Stiles, S. J. Bachofer and U. Simonis, *Langmuir*, 2002, **18**, 1030–1042.
51 A. R. Rakitin and G. R. Pack, *Langmuir*, 2005, **21**, 837–840.
52 J. Israelachvili, *Intermolecular and Surface Forces*, Academic Press, San Diego, 1991.
53 D. F. Evans and H. Wennerstrom, *The Colloidal Domain: Where Physics, Chemistry, Biology, and Technology Meet*, Wiley-VCH, New York, 2001.
54 D. Wang, R. H. Dong, P. F. Long and J. C. Hao, *Soft Matter*, 2011, **7**, 10713–10719.
55 H. Sakai, A. Matsumura, S. Yokoyama, T. Saji and M. Abe, *J. Phys. Chem. B*, 1999, **103**, 10737–10740.
56 D. H. Thompson, P. Shum and J. M. Kim, *Adv. Drug Delivery Rev.*, 2001, **53**, 273–284.
57 D. Danino, A. Bernheim-Groswasser and Y. Talmon, *Colloids Surf., A*, 2001, **183**, 113–122.

Electronic Supplementary Material (ESI) for Soft Matter
This journal is © The Royal Society of Chemistry 2013

Supporting Information for:

A Simple Route to Fluids with Photo-Switchable Viscosities Based on a Reversible Transition between Vesicles and Wormlike Micelles

Hyuntaek Oh, Aimee M. Ketner, Romina Heymann, Ellina Kesselman,
Dganit Danino, Daniel E. Falvey, and Srinivasa R. Raghavan

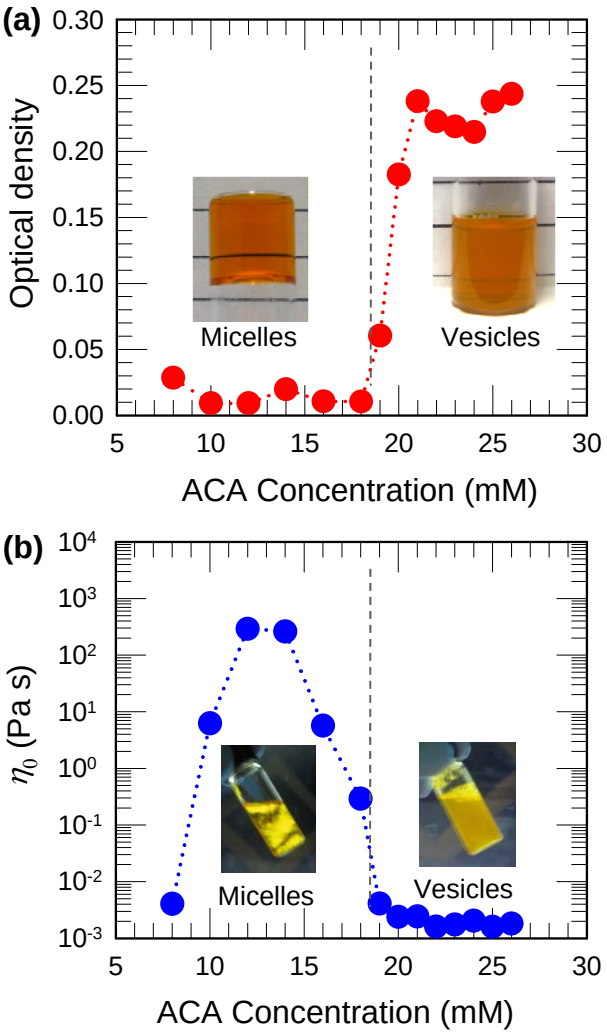

Figure S1. Phase behavior and rheology at 25°C of EHAC/ACA mixtures at a fixed [EHAC] of 40 mM and varying [ACA]. The molar ratio of NaOH to ACA is fixed at 1.1. The plot (a) shows the optical density at a wavelength of 700 nm, which quantifies the amount of light scattered from the sample. The plot (b) shows the zero-shear viscosity η_0 obtained from steady-shear rheology. Samples at [ACA] between 10 and 16 mM are transparent and highly viscous, as shown by the photograph of a sample resisting flow in an inverted vial (top left). These samples are also flow-birefringent, as shown by the photograph of a sample viewed under crossed polarizers while being shaken (bottom left). Together, the high viscosity and flow-birefringence point to the presence of wormlike micelles. In contrast, samples with [ACA] > 18 mM have a low viscosity close to water and are turbid, as can be noted from the photograph of a typical sample (top right). The same samples also do not show any flow-birefringence (photograph of a shaken sample under crossed-polarizers in bottom right). Together, the low viscosity and the turbidity point to the presence of vesicles.

This journal is © The Royal Society of Chemistry 2013

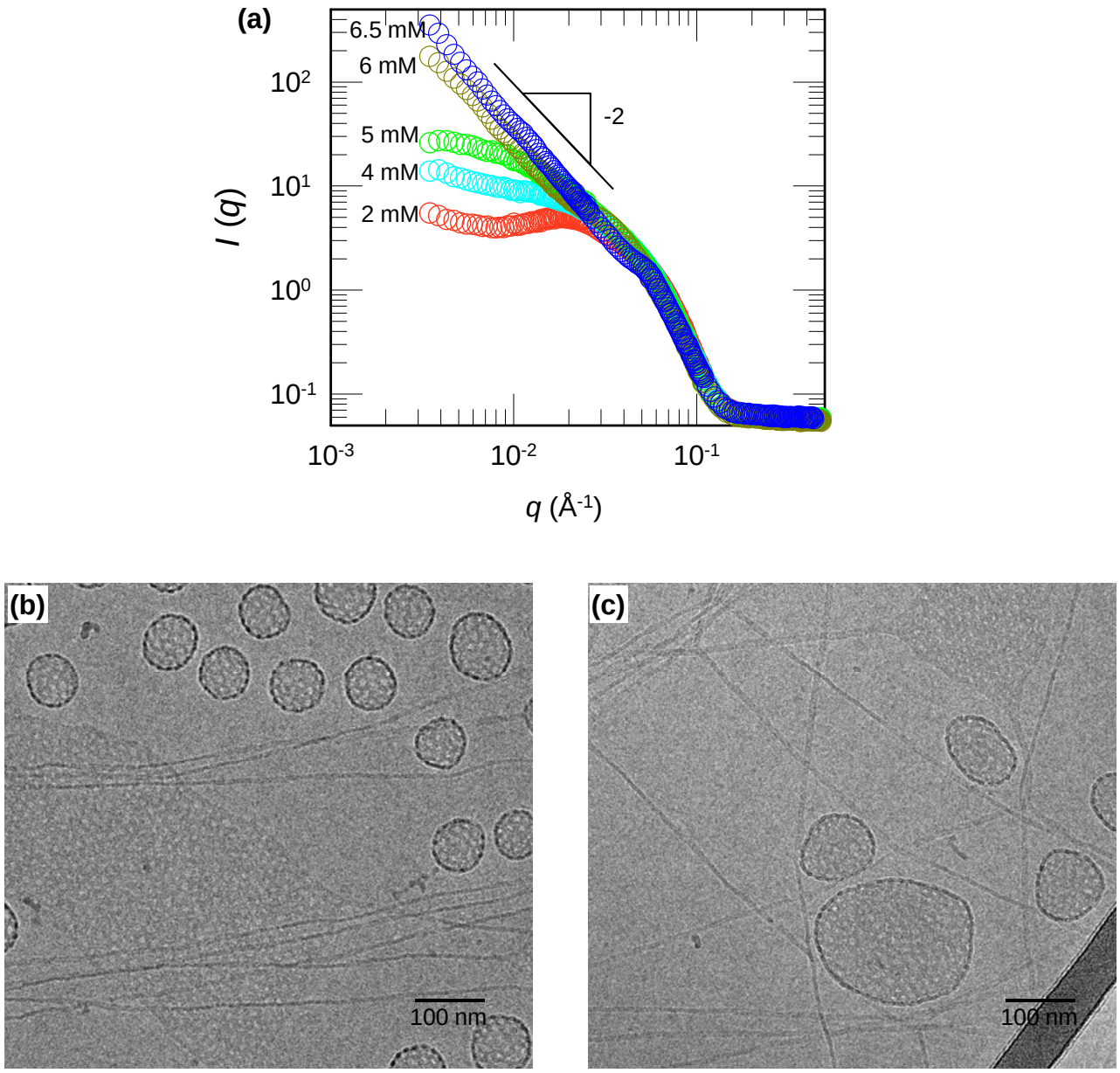

Figure S2. (a) SANS data at 25°C from EHAC/ACA mixtures in D_2O at a fixed [EHAC] of 10 mM with various ACA concentrations. The molar ratio of NaOH to ACA is fixed to 1.1. For ACA concentrations of 6 and 6.5 mM, *I* follows a slope of –2 at low *q*, which is indicative of scattering from vesicles. **(b), (c)** Cryo-TEM images of a sample containing 40 mM EHAC, 20 mM ACA, and 22 mM NaOH show mostly vesicle structures (see Figure 2d also). In some parts of the sample, stretched and interwoven wormlike micelles were also observed in rare cases, as seen in the above images.

This journal is © The Royal Society of Chemistry 2013

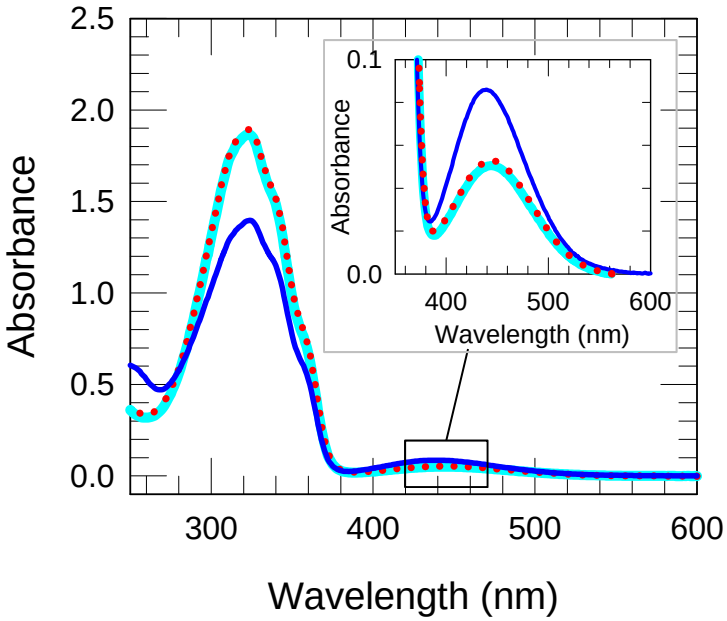

Figure S3. UV-Vis spectra of 40 mM EHAC, 20 mM ACA, and 22 mM NaOH before irradiation (cyan line), after UV irradiation for 1 h (blue line), and after subsequent visible light irradiation for 1.5 h (dotted red line). The sample was diluted 20 times with water. The changes at the visible wavelengths are enlarged and shown in the inset. UV irradiation causes a drop in absorbance at UV wavelengths and an increase in absorbance at visible wavelengths, indicating that ACA has been photoisomerized from *trans* to *cis*. Subsequent visible-light irradiation causes an increase in absorbance at the UV wavelengths and decrease at the visible wavelengths, indicating the reverse *cis* to *trans* photoisomerization.